INTERNATIONAL JOURNAL FOR NUMERICAL METHODS IN FLUIDS, VOL. 14, 1037–1062 (1992)

LAMINAR FLUID CONVECTION BETWEEN CONCENTRIC AND ECCENTRIC HEATED HORIZONTAL ROTATING CYLINDERS FOR LOW-PRANDTL-NUMBER FLUIDS

T. S. LEE

Mechanical and Production Engineering Department, Faculty of Engineering, National Universtiy of Singapore, 10 Kent Ridge Crescent, Singapore 0511

SUMMARY

Numerical experiments are performed to study rotational effects on the mixed convection of low-Prandtl-number fluids enclosed between the annuli of concentric and eccentric horizontal cylinders. The inner cylinder is assumed to be heated and rotating. The rotational Reynolds number considered is in the range where the effect of Taylor vortices is negligible. The Prandtl number of the fluid considered is in the range 0·01–1·0. The Rayleigh number considered is up to 10^6. A non-uniform mesh transformation technique coupled with the introduction of 'false transient' parameters to the vorticity and streamfunction–vorticity expressions was used to solve the governing set of equations. Results show that when the inner cylinder is made to rotate, the multicellular flow patterns observed in stationary cylindrical annuli subside in a manner depending on the Prandtl number of the fluids. Eventually the flow tends toward a uniform flow similar to that of a solid body rotation. For a fixed Rayleigh number and with a Prandtl number of the order of 1·0, when the inner cylinder is made to rotate, the mean Nusselt number is observed to decrease throughout the flow. For lower Prandtl number of the order 0·1–0·01 the mean Nusselt number remained fairly constant when the inner cylinder was made to rotate. The mean Nusselt numbers obtained were also compared with available data from other investigators.

KEY WORDS Eccentric cylinders Fluid convection Rotation Low-Prandtl-number fluids

INTRODUCTION

Heat transfer and fluid flow processes in enclosed spaces have been extensively studied because of their importance in energy conversion, storage and transmission systems. Stationary horizontal concentric and eccentric annular geometries are most commonly encountered in solar collector–receiver systems, cooling systems in nuclear reactors, etc. Comprehensive and extensive reivews of these works have been collated by Kuehn and Goldstein[1,2] and others.[3–9]

For mixed convection in the annulus between concentric or eccentric cylinders in a rotating system, most works have been performed for vertical cylindrical annuli.[10,11] Recently, rotational effects on natural convection in horizontal cylinders have become of interest to researchers.[12–17] Applications of these studies include food processing[18,19] and the interest in seeking improved methods for crystallographic-perfection industrial processes.[20,21] Most of the above studies are for air with $Pr = 0{\cdot}7$[12–16] or with concentric cylindrical annuli.[16,17] However, other effects of rotation on the heat transfer characteristics of low-Prandtl-number fluids are encountered in high-power electric machines with heated shafts, e.g. mercury slip-ring assemblies. This parameter was studied for a concentric case by Gardiner and Sabersky.[22] Experiments were performed at

0271–2091/92/091037–26$13.00

Received 3 February 1991
Revised 27 August 1991

three different Prandtl numbers of 2·5, 4·5 and 6·5 and at Taylor numbers (rotational Reynolds number) up to about 10^6. The results showed that the heat transfer coefficients generally increased with increasing Taylor number in a complex three-dimensional flow environment. The effects of varying Prandtl number on the velocity and temperature distributions were also studied by Singh and Rajvanshi[23] for different cylinder eccentricities. A bipolar co-ordinate system was used to solve the two-dimensional energy equation with the temperature expressed in the form of a perturbation function. Fusegi *et al.*[24] and Prud'homme and Robillard[19] considered mixed convection between concentric horizontal cylinders with the inner cylinder rotating at constant angular velocity. The numerical experiments were limited to a range of parameters (specified by $\sigma = Gr/Re^2$) that specifically excludes the appearance of Taylor vortices. In furtherance of these works, other studies have also been carried out on mixed natural convection in horizontal eccentric annuli by Ratzel *et al.*[25] and Projahn *et al.*[26]

The present study investigates the fluid motion and heat transfer characteristics of fluid with low Prandtl number of order 0·01–1·0 contained within a horizontal cylindrical annulus. Because of the excellent heat transfer characteristics of low-Prandtl-number fluids (e.g. liquid mercury), such fluids are increasingly being considered for use as the working fluid in several power-generating cycles. It is therefore of considerable importance to understand the convective fluid flow motion and heat transfer characteristics when such fluids are used. This low-Prandtl-number fluid flow situation also arises in cooling systems for electric motors of high power density and in the convective fluid motion in a heated cylinder with a mercury slip-ring assembly. For the present problem, where natural convection is driven by a vertical temperature gradient and vertical gravity force, the interaction with the effect of high rotational rate of the inner cylinder will be expected to lead to complicated three-dimensional flows with Taylor vortices. Here we purposely limited the calculations to a range of parameters that would exclude this possibility.

GOVERNING EQUATIONS

A schematic configuration of the eccentric annulus is shown in Figure 1. The inner cylinder is assumed to be heated and rotating. Flow in the annular region is assumed to be two-dimensional, steady and laminar, with an absence of Taylor vortices. The governing equations which describe the fluid motion of the incompressibe fluid between the annulus, based on the Boussinesq approximation, are then given by:

momentum equation,

$$\frac{\mathrm{D}\mathbf{u}}{\mathrm{D}t} = -\frac{\nabla p}{\rho_R} - \beta(T - T_R)\mathbf{g} + \nu\nabla^2\mathbf{u}; \tag{1}$$

continuity equation,

$$\nabla \cdot \mathbf{u} = 0; \tag{2}$$

energy transport equation,

$$\frac{\mathrm{D}T}{\mathrm{D}t} = \alpha\nabla^2 T. \tag{3}$$

Using the vector identity

$$(\nabla \times \mathbf{u}) \times \mathbf{u} = \mathbf{u} \cdot \nabla\mathbf{u}^2/2,$$

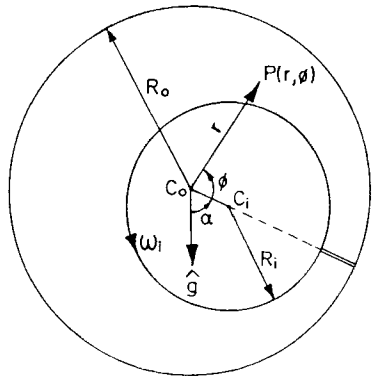

(a)

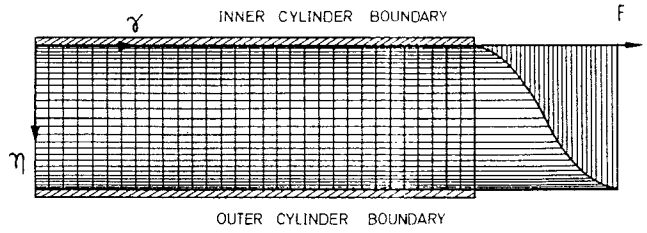

(b)

Figure 1. (a) Co-ordinate system in eccentric annular flow region. (b) Non-uniform computational mesh in transformed domain

taking the curl of (1) and invoking (2), the resulting equation is

$$\frac{\partial \zeta}{\partial t} - \nabla \times (\mathbf{u} \times \zeta) = -\beta \nabla \times (T - T_R)\mathbf{g} + \nu \nabla^2 \zeta, \tag{4}$$

with the vorticity vector given by

$$\zeta = \nabla \times \mathbf{u}. \tag{5}$$

We introduce the dimensionless variables $r^* = r/L$, $t^* = t/(L^2/\alpha)$, $u^* = u/(\alpha/L)$, $v^* = v/(\alpha/L)$, $\zeta^* = \zeta/(\alpha/L^2)$, $\psi^* = \psi/\alpha$ and $\theta = (T - T_R)/T_m$, where r^*, t^*, u^*, v^*, ψ^* and θ represent the dimensionless radial co-ordinate, time, radial velocity, tangential velocity, streamfunction and temperature respectively. With $T_R = (T_i + T_o)/2$ and $T_m = (T_i + T_o)/2$, equations (3) and (4) give

$$\frac{\partial \theta}{\partial t} + \mathbf{u}^2 \cdot \nabla \theta = \nabla^2 \theta, \tag{6}$$

$$\frac{\partial \zeta}{\partial t} - \nabla \times (\mathbf{u} \times \zeta^*) = -Ra\, Pr(\nabla \times \theta \mathbf{g}) + Pr(\nabla^2 \zeta^*), \tag{7}$$

where all variables are now in dimensionless form. $Ra = gL^3 T_m / \nu\alpha$ is the Rayleigh number and $Pr = \nu/\alpha$ is the Prandtl number.

With the vorticity vector defined by (5), the streamfunction vector $\boldsymbol{\psi}$ is defined such that a ψ-isoline is a streamline, i.e.

$$\mathbf{u} = \nabla \times \boldsymbol{\psi}^* \tag{8}$$

Substituting (8) into (5) gives

$$\boldsymbol{\zeta}^* = \nabla \times (\nabla \times \boldsymbol{\psi}^*), \tag{9}$$

and since $\boldsymbol{\psi}^*$ is required to be solenoidal,

$$\nabla \cdot \boldsymbol{\psi}^* = 0. \tag{10}$$

It can be shown that (9) can be written as a vector Poisson equation

$$\boldsymbol{\zeta}^* = -\nabla^2 \boldsymbol{\psi}^*. \tag{11}$$

(From hereon the superscript asterisks representing dimensionless quantitites are dropped for simplicity.)

The steady state solution of (6), (7) and (11) may be obtained by an iterative procedure, e.g. Jacobi iteration, or by various relaxation methods.[27] If the latter approach is used, then for each overall iteration loop of the set of steady state equations ($\partial/\partial t = 0$) there will be as many inner iteration loops as there are equations. Each of these inner iteration loops has to converge before the next overall iteration loop can be performed. For the set of steady state form (6), (7) and (11) this procedure can become very time-consuming. An improved method is to approach the steady state solution through the corresponding unsteady equations

$$\frac{\partial \theta}{\partial t} + \mathbf{u} \cdot \nabla \theta = \nabla^2 \theta, \tag{12}$$

$$\frac{\partial \boldsymbol{\zeta}}{\partial t} - \nabla \times (\mathbf{u} \times \boldsymbol{\zeta}) = -Ra\, Pr(\nabla \times \theta \mathbf{g}) + Pr(\nabla^2 \boldsymbol{\zeta}), \tag{13}$$

where t is dimensionless time.

This time-dependent transient approach to the steady state solution is attractive. If there is more than one equation of the vorticity–transport type, then most of the inner iteration loops are eliminated. Unfortunately, (11) remains elliptic in form. Its numerical solution requires an iterative technique at each time step to determine the streamfunction at that time. The overall solution process is then multi-iterative.

For the problems considered here we are only interested in the steady state solutions. The inner iteration loop of the streamfunction–vorticity equation $\boldsymbol{\zeta} = -\nabla^2 \boldsymbol{\psi}$ seems an unnecessary burden in terms of computing effort. If the steady state solution is unique and is independent of the transient approach to it, then the steady state solution of (8)–(11) can be reached by introducing a transient term into the streamfunction–vorticity equation and treating the streamfunction as a transport quantity:

$$\frac{\partial \boldsymbol{\psi}}{\partial t} = \nabla^2 \boldsymbol{\psi} + \boldsymbol{\zeta}. \tag{14}$$

Numerical experimentation shows that the stability characteristics of (12)–(14) vary according to the relative magnitudes of the source terms in the respective equations; also, convective stability of the flow does not affect (14). In terms of numerical stability with a fixed time increment

Δt and fixed mesh sizes, (14) was found to be the most stable and the vorticity transport equation (13) is numerically most unstable. Hence some 'false transient' terms are introduced into equation (14) to 'speed up' the solution and into equation (13) to stabilize the solution for a fixed time increment. The steady state solution is finally obtained through a set of 'fast and stable' transient equations

$$\frac{1}{\alpha_\psi}\frac{\partial \psi}{\partial t}=\nabla^2\psi+\zeta, \tag{15}$$

$$\frac{\partial \theta}{\partial t}+\mathbf{u}\cdot\nabla\theta=\nabla^2\theta, \tag{16}$$

$$\frac{1}{\alpha_\zeta}\frac{\partial \zeta}{\partial t}-\nabla\times(\mathbf{u}\times\boldsymbol{\zeta})=-RaPr(\nabla\times\theta\mathbf{g})+Pr(\nabla^2\boldsymbol{\zeta}). \tag{17}$$

For two-dimensional problems in cylindrical polar co-ordinates (15)–(17) may be written as

$$\frac{1}{\alpha_\psi}\frac{\partial \psi}{\partial t}=\frac{\partial^2\psi}{\partial r^2}+\frac{1}{r}\frac{\partial \psi}{\partial r}+\frac{1}{r^2}\frac{\partial^2\psi}{\partial \phi^2}+\zeta, \tag{18}$$

$$\frac{\partial \theta}{\partial t}+u\frac{\partial \theta}{\partial r}+\frac{v}{r}\frac{\partial \theta}{\partial \phi}=\frac{\partial^2\theta}{\partial r^2}+\frac{1}{r}\frac{\partial \theta}{\partial r}+\frac{1}{r^2}\frac{\partial^2\phi}{\partial \phi^2}, \tag{19}$$

$$\frac{1}{\alpha_\zeta}\frac{\partial \zeta}{\partial t}+u\frac{\partial \zeta}{\partial r}+\frac{v}{r}\frac{\partial \zeta}{\partial \phi}=Pr\left(\frac{\partial^2\zeta}{\partial r^2}+\frac{1}{r}\frac{\partial^2\zeta}{\partial r^2}+\frac{1}{r^2}\frac{\partial^2\zeta}{\partial \phi^2}\right)+RaPr\left(\sin\phi\frac{\partial \theta}{\partial r}+\frac{1}{r}\cos\phi\frac{\partial \theta}{\partial \phi}\right). \tag{20}$$

The velocities given by a streamfunction ψ in dimensionless form are

$$u=\frac{1}{r}\frac{\partial \psi}{\partial \phi}, \qquad v=-\frac{\partial \psi}{\partial r}. \tag{21}$$

The values of α_ψ lies between 1·0 and 10 and the values of α_ζ lies between 0·0 and 1·0. The time step used in the numerical solution follows the Courant–Ferderic–Lewis conditions.

GOVERNING EQUATIONS IN TRANSFORMED SPACED

Figure 1(a) shows the co-ordinate system of the annulus with an eccentricity $C_iC_o=\varepsilon$ at an angle α to the vertical axis. The transformed solution region ($0\leqslant\eta\leqslant1$, $0\leqslant\gamma\leqslant2\pi$) is shown in Figure 1(b). The lines with constant η in the transformed solution region correspond to eccentric circles in the original solution region of Figure 1(a). In the transformed solution region (η, γ) is defined as

$$\eta=\frac{r-r_i}{r_o-r_i}=f(r,\phi), \qquad \gamma=(\gamma_{ref}-\alpha)+\phi, \tag{22}$$

where

$$r_o=R_o, \qquad r_i=\varepsilon\cos\phi+[(\varepsilon\cos\phi)^2+R_i^2-\varepsilon^2]^{1/2} \quad \text{for } \varepsilon+R_i<R_o \text{ and } \varepsilon<R_i.$$

By replacing all the partial derivatives in (18)–(21) with partial derivatives with respect to the transformed variable, the (dimensionless) equations become

$$\frac{1}{\alpha_\psi}\frac{\partial \psi}{\partial t}+\left(\beta^2+\frac{\kappa^2}{r^2}\right)\frac{\partial^2\psi}{\partial \eta^2}+\left(\frac{\beta}{r}+\frac{\lambda}{r^2}\right)\frac{\partial \psi}{\partial \eta}+\frac{2}{r^2}\frac{\partial^2\psi}{\partial \gamma\partial \eta}+\frac{1}{r^2}\frac{\partial^2\psi}{\partial \gamma^2}+\zeta, \tag{23}$$

$$u=\frac{1}{r}\frac{\partial\psi}{\partial\gamma}+\frac{\kappa}{r}\frac{\partial\psi}{\partial\eta}, \tag{24}$$

$$v=-\beta\frac{\partial\psi}{\partial\eta}, \tag{25}$$

$$\frac{\partial\theta}{\partial t}+\left(u\beta+\frac{\kappa v}{r}\right)\frac{\partial\theta}{\partial\eta}+\frac{v}{r}\frac{\partial\theta}{\partial\gamma}=\left(\beta^2+\frac{\kappa^2}{r^2}\right)\frac{\partial^2\theta}{\partial\eta^2}+\left(\frac{\beta}{r}+\frac{\lambda}{r^2}\right)\frac{\partial\theta}{\partial\eta}+\frac{2\kappa}{r^2}\frac{\partial^2\theta}{\partial\eta\partial\gamma}+\frac{1}{r^2}\frac{\partial^2\theta}{\partial\gamma^2}, \tag{26}$$

$$\frac{1}{\alpha_\zeta}\frac{\partial\zeta}{\partial t}+\left(u\beta+\frac{\kappa v}{r}\right)\frac{\partial\zeta}{\partial\eta}+\frac{v}{r}\frac{\partial\zeta}{\partial\gamma}=Pr\left(\beta^2+\frac{\kappa^2}{r^2}\right)\frac{\partial^2\zeta}{\partial\eta^2}+Pr\left(\frac{\beta}{r}+\frac{\lambda}{r^2}\right)\frac{\partial\zeta}{\partial\eta}+\frac{2Pr\kappa}{r^2}\frac{\partial^2\zeta}{\partial\eta\partial r}+\frac{Pr}{r^2}\frac{\partial^2\zeta}{\partial\gamma^2}$$
$$+RaPr\left(\beta\sin\gamma+\frac{\kappa\cos\gamma}{r}\right)\frac{\partial\theta}{\partial\eta}+\frac{RaPr\cos\gamma}{r}\frac{\partial\theta}{\partial\gamma}. \tag{27}$$

BOUNDARY CONDITIONS

At the boundaries ψ is constant since there is no flow across the boundaries, i.e.

$$\psi(\eta=1)=\psi_o=0, \qquad \psi(\eta=0)=\psi_i=f(Re), \tag{28}$$

where $f(Re)$ is determined by the requirement that the pressure distribution be single-valued.

With the inner cylinder rotating at an angular velocity ω corresponding to a rotational Reynolds number $Re=R_i\omega L/\nu$ and assuming no slip at the boundaries, we have

$$u(\eta=0)=0, \qquad u(\eta=1)=0, \qquad v(\eta=0)=RePr, \qquad v(\eta=1)=0. \tag{29}$$

θ at the boundaries is given by

$$\theta(\eta=0)=1, \qquad \theta(\eta=1)=-1. \tag{30}$$

At the inner and outer boundaries $\psi=$constant, hence

$$\zeta=-\beta^2\frac{\partial^2\psi}{\partial\eta^2}+\frac{v}{r}. \tag{31}$$

NUMERICAL METHODS

The solution region in Figure 1(a) is 'cut' along the $\gamma=\gamma_{ref}$ radial line and stretched into a rectangular γ–η domain as defined by equation (22) and shown in Figure 1(b). In order to obtain better resolution of the solution near the wall regions while preserving the second-order accuracy of the finite difference scheme, the continuous rectangular domain is then overlayed with a non-uniform finite difference mesh generator as shown in Figure 1(b) and given by

$$F=\frac{2}{\pi}\sin^{-1}(\eta^{1/2}). \tag{32}$$

At the node points the finite difference solutions to (23)–(31) with their boundary conditions are obtained. The numerical procedure used involves an alternating direction implicit (ADI) method originally proposed by Peaceman and Rachford[28] which is modified here by the inclusion of a weighted time step factor σ and the false transient parameter α_ζ.

For the vorticity transport equation the advancement over one time step is accomplished

through

$$\begin{aligned}(I-\sigma\alpha_\zeta\Delta t\,A_\gamma)(\zeta)^*&=(A_\gamma+A_\eta)(\zeta)^n+(S_D)^n,\\(I-\sigma\alpha_\zeta\Delta t\,A_\eta)(\zeta)^{**}&=(\zeta)^*,\\(\zeta)^{n+1}&=(\zeta)^n+\Delta t(\zeta)^{**},\end{aligned}\tag{33}$$

where $(\zeta)^*$ and $(\zeta)^{**}$ are dummy variables, A_γ and A_η are matrix operators formed through finite differencing of the governing equations in the γ- and η-direction respectively, $(S_D)^n$ is the source term evaluated at the most recent solution field and I is an identity matrix. This scheme is equivalent to

$$\frac{(\zeta)^{n+1}-(\zeta)^n}{\alpha_\zeta\Delta t}=(A_\gamma+A_\eta)(1-\sigma)(\zeta)^n+(A_\gamma+A_\eta)\sigma(\zeta)^{n+1}-\sigma^2(A_\gamma A_\eta)[(\zeta)^{n+1}-(\zeta)^n]+(S_D)^n.\tag{34}$$

For $\sigma=\frac{1}{2}$ the above scheme corresponds to the Crank–Nicholson equation.

The same method is adopted in solving the temperature and streamfunction–vorticity equations. All spatial derivatives are approximated by second-order-accurate central differences. The convective terms in (19) and (20) are approximated by using a second-order upwind differencing method. The mixed spatial derivatives resulting from the mesh transformation are handled by the method proposed by McKee and Mitchell.[29] The resulting linear set of finite difference equations is then solved by an algorithm due to Thomas (see Reference 27). Three-point backward and forward difference formulae are used for derivatives at the boundaries.

The streamfunction ψ_o on the outer cylinder wall is arbitrarily set to zero. For the stationary inner cylinder the streamfunction ψ_i on the inner cylinder wall is set equal to the outer cylinder streamline value. This is because the rising plume touches the outer cylinder wall and the net circulating volumetric flow rate round the cylinders is zero when the inner cylinder is not rotating. When the inner cylinder is made to rotate, the streamline value at the inner rotating cylinder wall, ψ_i, cannot be preassigned. The use of $\partial\psi/\partial n=$ wall velocity gives a solution for which $\partial\psi/\partial s\neq 0$ along the wall of the inner cylinder. This implies that fluid was numerically 'leaked' through the moving inner cylinder wall. In the present study ψ_i is determined using the criterion that the pressure distribution in the solution region is a single-valued function. Mathematically, this criterion implies that the line integral of the pressure gradient $\partial P/\partial s$ along any closed loop circumscribing the inner cylinder is zero, i.e. $\oint(\partial P/\partial s)\,ds=0$. $\partial P/\partial s$ can be evaluated from the momentum conservation equations.

The finite difference boundary vorticity values are obtained by considering the Taylor series expansion of ψ into the solution region and taking into consideration the values of ψ and velocity at the boundary through (31), i.e.

$$\zeta_{i,1}=\frac{-2\beta^2}{(\Delta\eta)^2}\left(\psi_{i,2}-\psi_{i,1}+\frac{v}{\beta}\bigg|_{i,1}\Delta\eta\right)+\frac{v}{r}\bigg|_{i,1},\tag{35}$$

$$\zeta_{i,N}=-2\beta^2\frac{\psi_{i,N-1}}{(\Delta\eta^2)},\tag{36}$$

where the inner cylinder wall node point is at $j=1$ and the outer cylinder wall node point is at $j=N$.

The heat transfer at the inner cylinder wall is defined by the local Nusselt number

$$Nu=-\frac{\partial\theta}{\partial r}=-\beta\frac{\partial\theta}{\partial\eta}.\tag{37}$$

The average Nusselt number is then determined from

$$\overline{Nu} = \int_0^{2\pi} Nu \, d\gamma/2\pi. \tag{38}$$

The mean Nusselt number is also used as the quantity to indicate steady state convergence. The mean Nusselt number is computed at every 20th iteration. The steady state criterion is said to have been satisfied when a difference of less than 0·1% of a reference Nusselt number is detected. The computation of the Nusselt number requires differentiation of the temperature function and should therefore converge at a lower rate than the latter. This has proven satisfactory. The streamfunction, velocity, temperature and voriticity fields are noted to be steady when the Nusselt number is steady.

RESULTS

The discussion here is based on the steady state results obtained from the false transient solutions of the governing equations with initial values of ψ, u, v, θ and ζ all set to zero, except the temperatures at the inner and outer cylinder walls. The temperature is $+1$ at the inner wall and -1 at the outer wall. The solutions were initially tested with time steps of 0·1, 0·01, 0·001 and 0·0001 and mesh sizes of 21×41, 41×81, 81×161 and 161×321. It was found that variations in the solution fields were not significant (of the order of 0·1% in the temperature field, 0·1% in the streamline field, 0·2% in the vorticity field and 0·1% in the mean Nusselt number obtained) between time steps of 0·001 and 0·0001 and mesh sizes of 81×161 and 161×321. Hence for the results obtained here a dimensionless time increment of 0·001 and a mesh size of 81×161 were used.

With the above time step and mesh size the model was initially tested for validity with stationary cylinders of concentric configurations, for which data from other investigators are readily available for comparison. The numerical results of Ra versus $\overline{Nu}$ at radius ratios RR = 1·25, 2·6 and 5·0 are shown in Figure 2. Converted experimental data of Kuehn and Goldstein[1,2] for RR = 2·6 are also shown. The correlation curves of Raithby and Holland[30] for RR = 2·6 and 1·25 and the numerical results of Yang *et al.*[20,21] for RR = 1·4 and 2·6 and of Projahn *et al.*[26] for RR = 2·6 are also plotted in the same figure. The present numerical experiments indicate very good agreement with all these results.

Figure 3 shows the effects of vertical eccentricity on the flow and temperature distributions at $Ra = 10^5$, $Pr = 1{\cdot}0$, 0·1 and 0·01, RR = 2·6 and $Re = 0$ for vertical eccentricities $\varepsilon_v = \frac{2}{3}, \frac{1}{3}, -\frac{1}{3}, -\frac{2}{3}$. The immediate effect of displacing the inner cylinder downwards is to increase the convective region above the inner cylinder. Figure 3(a) shows that for $Pr = 1{\cdot}0$ the single thermal plume above the inner cylinder is enhanced when the inner cylinder is displaced downwards. For Prandtl number of 0·1–0·01 the bithermal plumes observed at some vertical eccentric locations are eliminated when the inner cylinder is displaced downwards (Figures 3(a) and 3(b)). Figure 4 shows the corresponding horizontal displacement of the inner cylinder from $\varepsilon_h = -\frac{2}{3}$ to $\varepsilon_h = \frac{2}{3}$. This has the effect of 'squeezing' the flow cells in the direction of the eccentricities and creating an 'open space' for the enhancement of the convective fluid motion. Further numerical experiments show that if the Rayleigh number is small ($Ra \leqslant 10^3$), no convective motion can take place for any value of the Prandtl number. The mean Nusselt number and the isotherm plots resemble those of pure conduction. The isotherms form concentric circles surrounding the inner cylinder. As the Rayleigh number increases, the convective strength increases. When the convective flow becomes strong enough, temperature inversion begins to take place and the basic counter-rotating pair of 'crescent-shaped' cells will be modified. The extent to which and the manner in which the

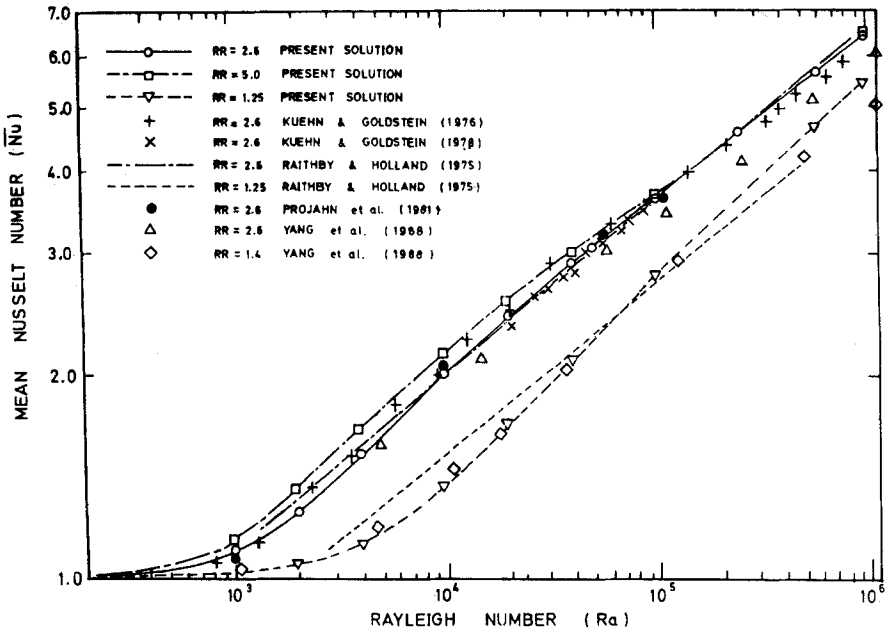

Figure 2. Mean Nusselt number versus Rayleigh number at various radius ratios (eccentricity $\varepsilon = 0{\cdot}0$)

modifications of the basic flow patterns take place depend very much on the Rayleigh number, Prandtl number and radius ratio as well as on the eccentricity of the inner cylinder. In general, it is observed that the convective mode of heat transfer is enhanced when eccentricity is introduced to the inner cylinder.

When the inner cylinder is made to rotate, the corresponding flow and temperature fields are as shown in Figures 5 and 6. A general trend is observed. With the inner cylinder rotating in the counterclockwise direction, any cell on the right of the inner cylinder will be dragged upwards by the viscous drag. At the same time, any cell on the left of the inner cylinder is dragged downwards by the viscous action of the inner cylinder rotation. The isotherms are thus tilted in the direction of rotation from the corresponding stationary cases. The degree of destruction of the left-hand cell and the degree of enhancement of the right-hand cell depend greatly on the basic flow. For a given Rayleigh number the general effect of tilting the thermal plume in the direction of rotation is more pronounced at higher Prandtl number. At higher rotational Reynolds number the convective strength as compared with the viscous drag induced by rotation is negligible. The immediate effect of rotating the inner cylinder is to set up a Couette-like rotation where all the fluid within the same annular spaces is rotating with virtually the same speed. These Couette-like flows are in the form of concentric circles surrounding the inner cylinder. The thermal plume tends to diffuse and the isotherms form circular rings surrounding the inner cylinder, suggesting that the mode of heat transfer is dominated by conduction.

For low-Prandtl-number fluid flow, as mentioned above and shown in Figures 3 and 4, a symmetrical bithermal plume was observed above the inner cylinder at certain eccentricities. The flow pattern in the annulus is observed to be multicellular in these cases. The heat transfer characteristics for these fluid flows with low Prandtl number were found to have points of maximum and minimum at the interior nodes, instead of at the top and bottom nodes which is

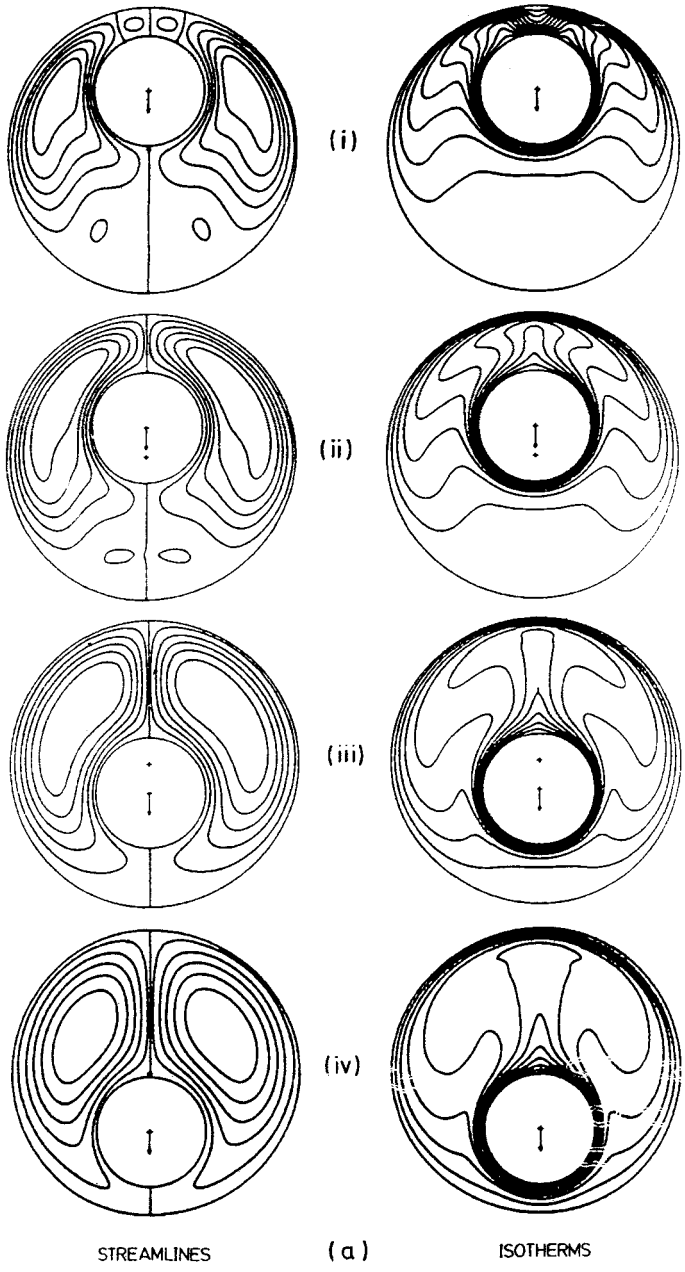

Figure 3. Streamlines and isotherms at various vertical eccentricities (RR = 2·6, $Ra = 10^5$, $Re = 0$): (a) $Pr = 1{\cdot}0$; (b) $Pr = 0{\cdot}1$; (c) $Pr = 0{\cdot}01$; (i) $\varepsilon_v = \frac{2}{3}$; (ii) $\varepsilon_v = \frac{1}{3}$; (iii) $\varepsilon_v = -\frac{1}{3}$; (iv) $\varepsilon_v = -\frac{2}{3}$

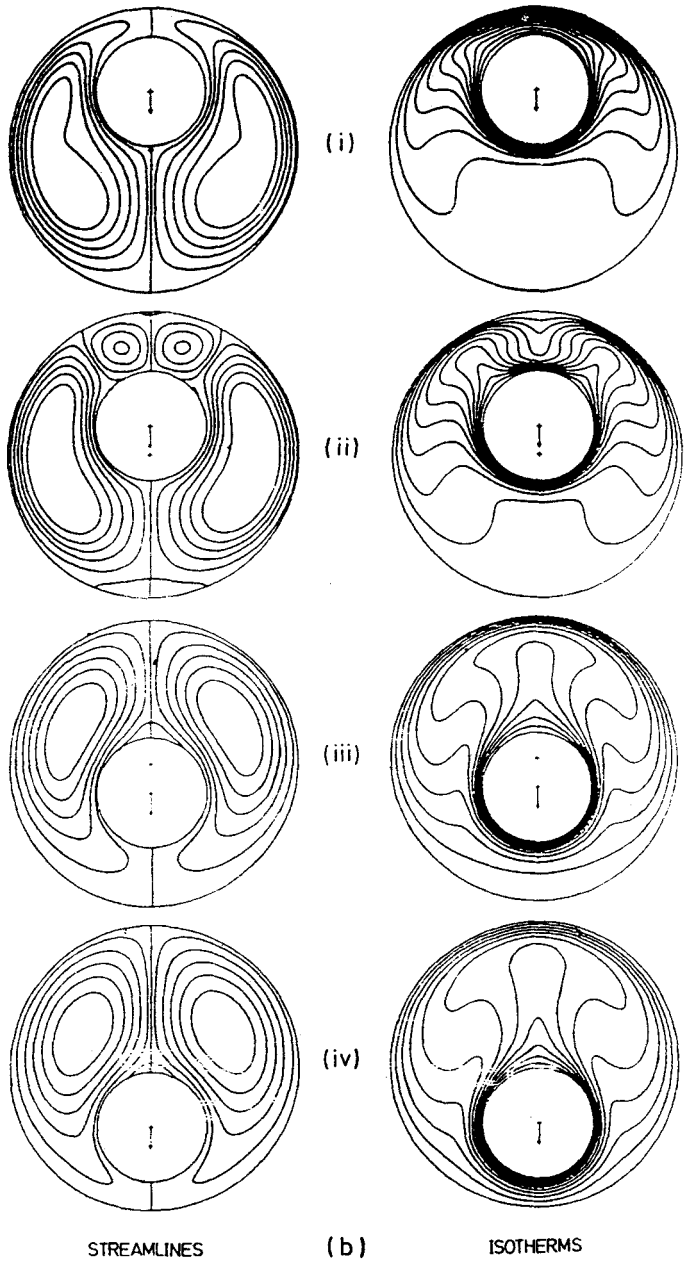

Figure 3. (Continued)

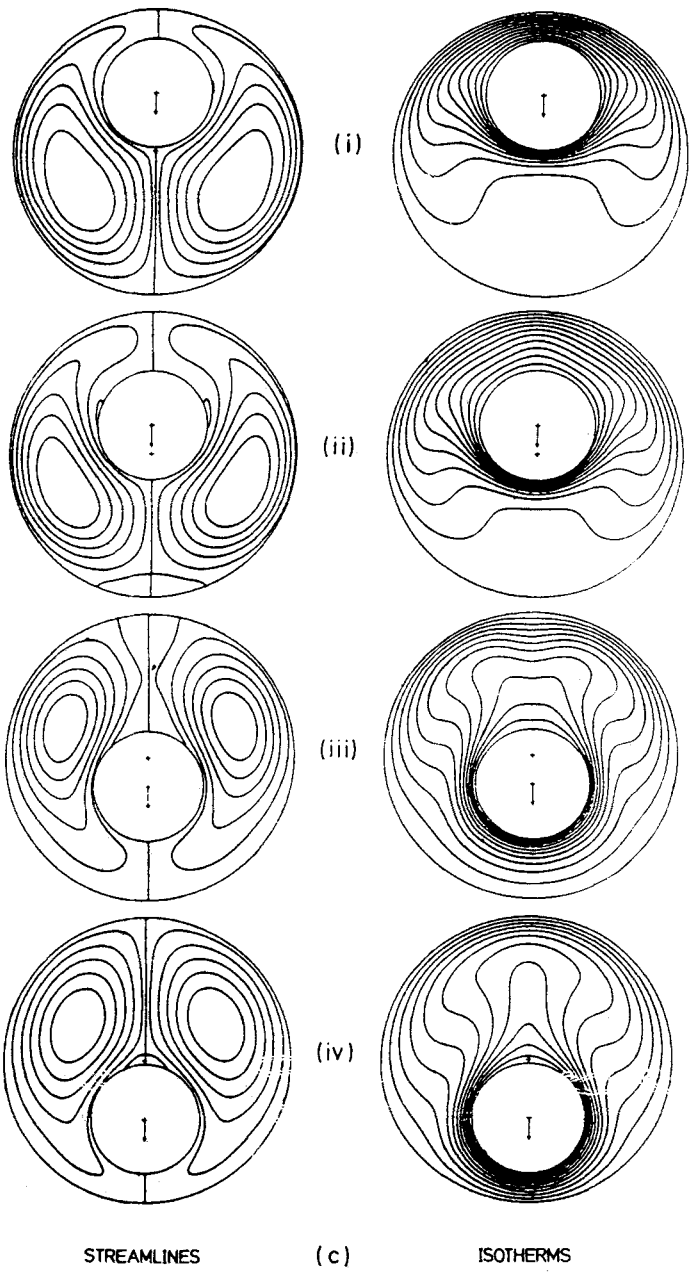

Figure 3. (Continued)

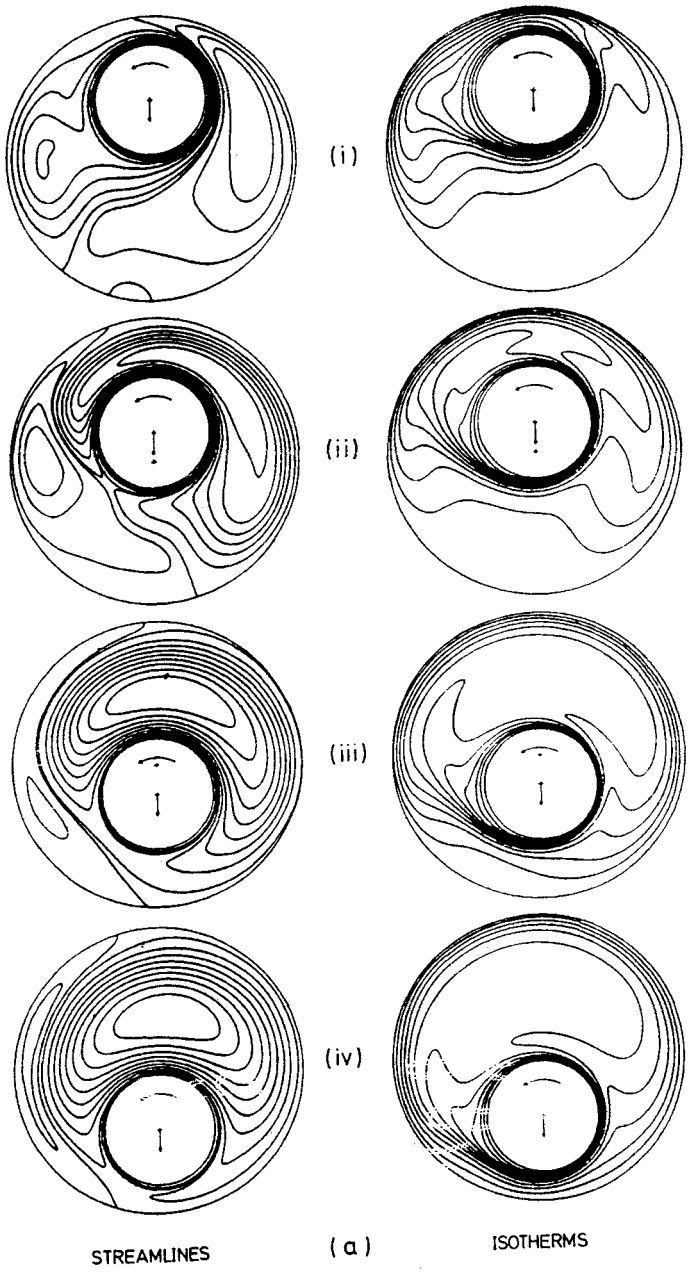

Figure 4. Streamlines and isotherms at various horizontal eccentricities (RR = 2·6, $Ra = 10^5$, $Re = 0$): (a) $Pr = 1{\cdot}0$; (b) $Pr = 0{\cdot}1$; (c) $Pr = 0{\cdot}01$; (i) $\varepsilon_h = -\frac{2}{3}$; (ii) $\varepsilon_h = 0{\cdot}0$; (iii) $\varepsilon_h = \frac{2}{3}$

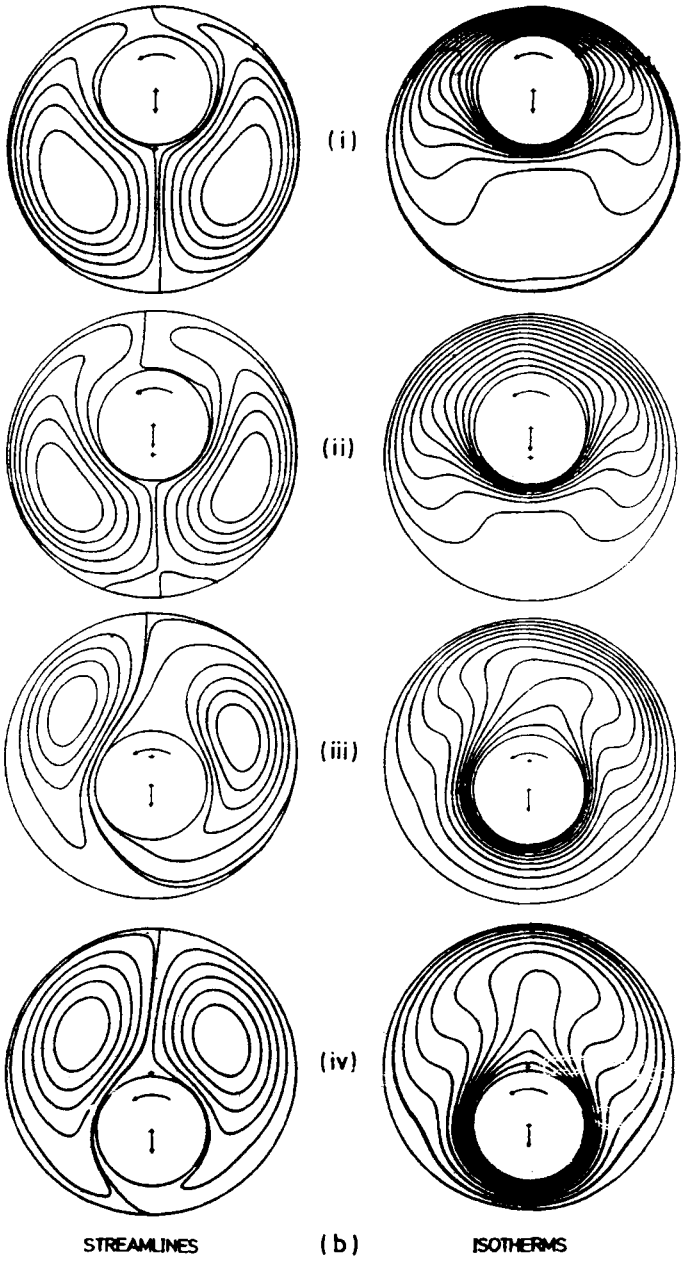

Figure 4. (Continued)

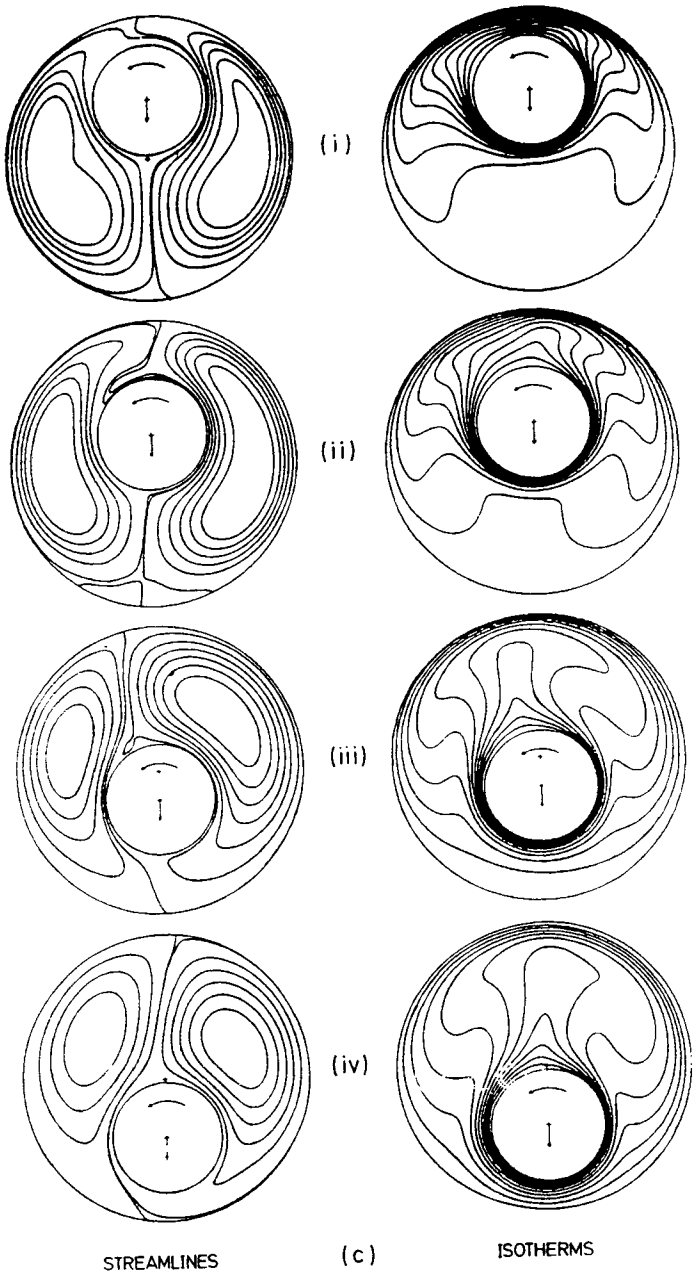

Figure 4. (Continued)

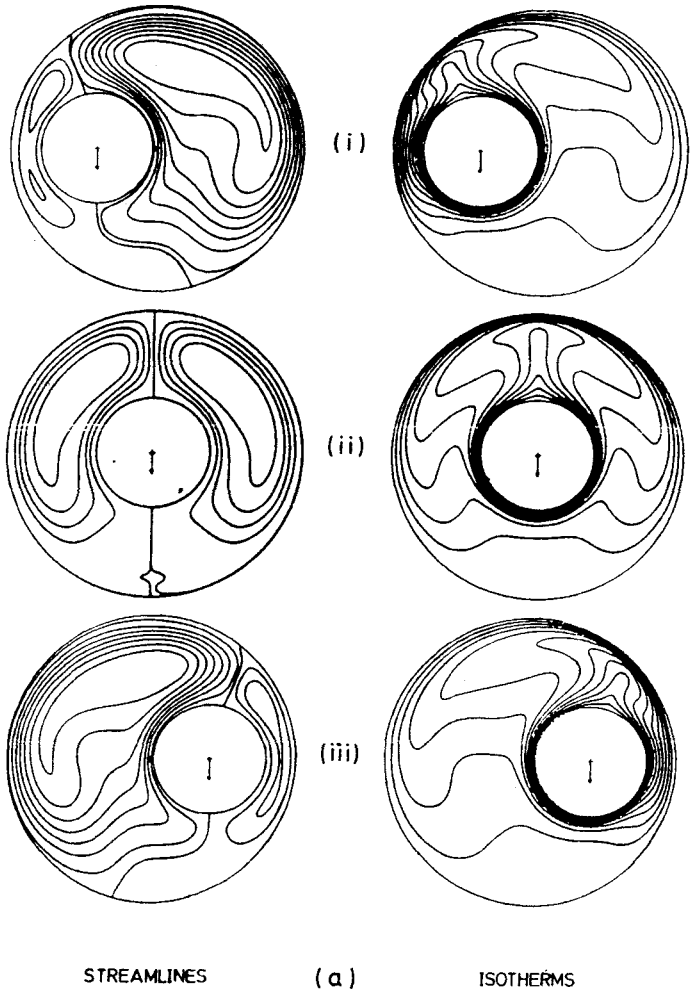

Figure 5. Inner cylinder rotation with various vertical eccentricities (RR = 2·6, $Ra = 10^5$, $Re = 560$): (a) $Pr = 1{\cdot}0$; (b) $Pr = 0{\cdot}1$; (c) $Pr = 0{\cdot}01$; (i) $\varepsilon_v = \frac{2}{3}$; (ii) $\varepsilon_v = \frac{1}{3}$; (iii) $\varepsilon_v = -\frac{1}{3}$; (iv) $\varepsilon_v = -\frac{2}{3}$

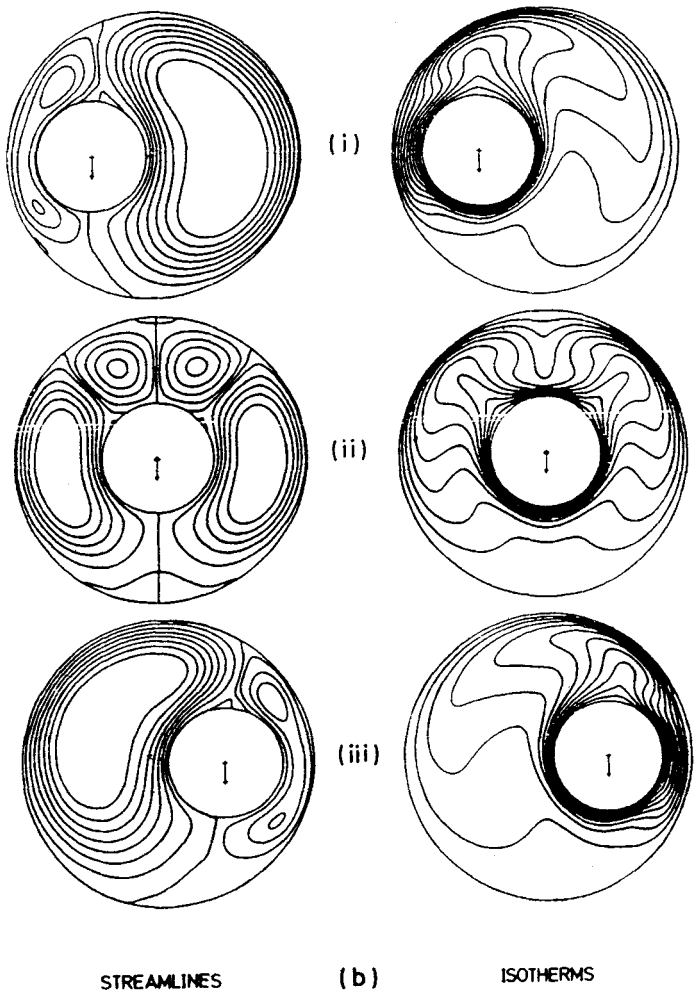

Figure 5. (Continued)

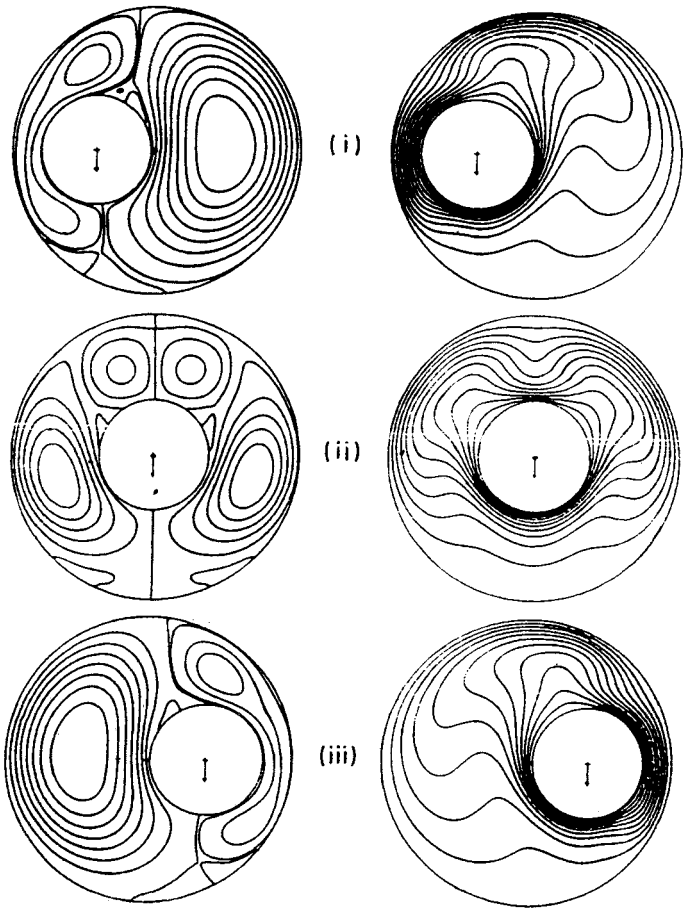

Figure 5. (Continued)

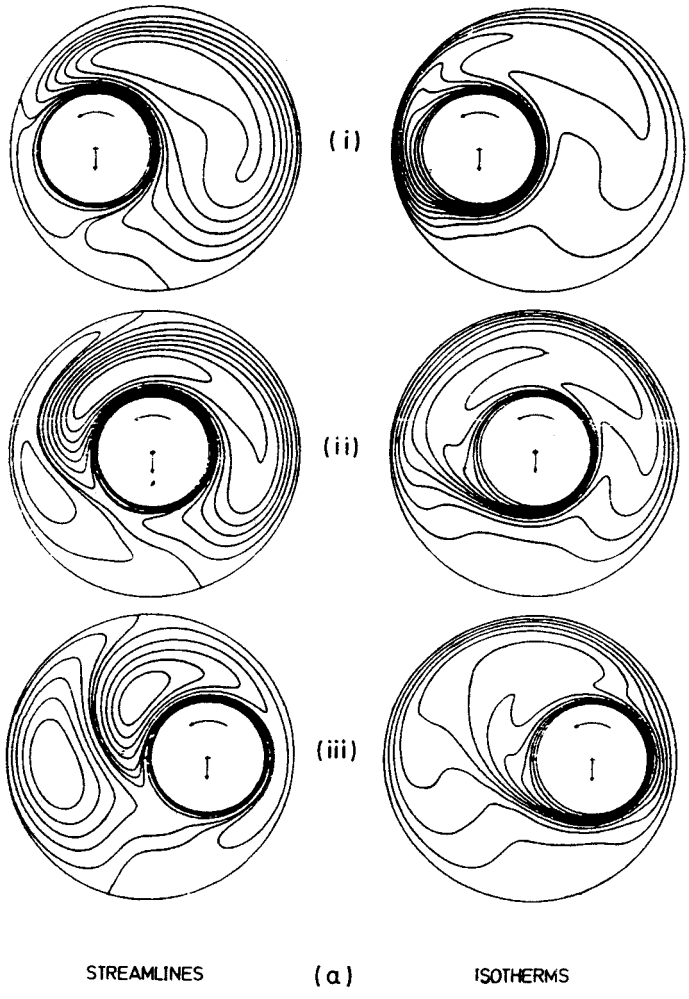

Figure 6. Inner cylinder rotation with various horizontal eccentricities (RR = 2·6, $Ra = 10^5$, $Re = 560$): (a) $Pr = 1{\cdot}0$; (b) $Pr = 0{\cdot}1$; (c) $Pr = 0{\cdot}01$; (i) $\varepsilon_h = -\frac{2}{3}$; (ii) $\varepsilon_h = 0{\cdot}0$; (iii) $\varepsilon_h = \frac{2}{3}$

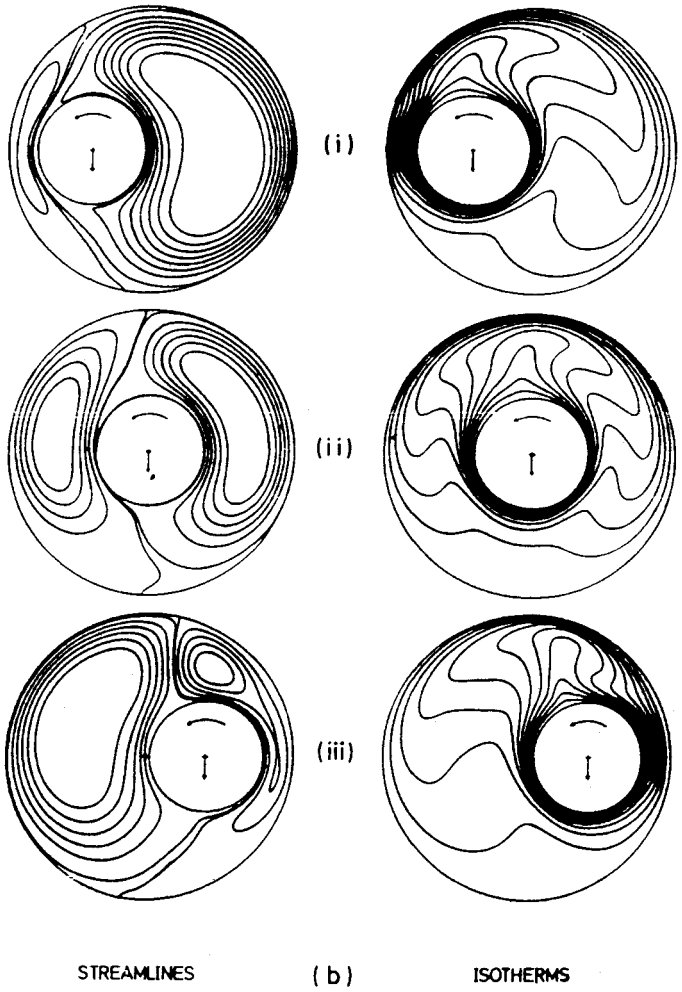

Figure 6. (Continued)

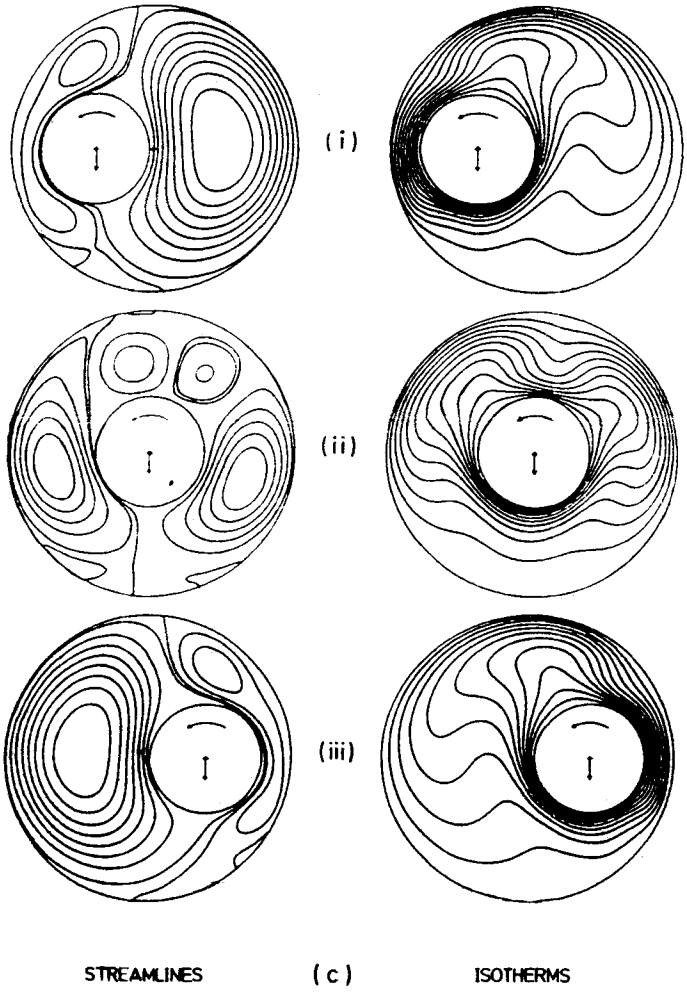

Figure 6. (Continued)

known for high-Prandtl-number fluids. When the inner cylinder is made to rotate, the flow pattern becomes more complex (Figures 5 and 6). The multicellular flow with its bithermal plume on one side of the annulus for low-Prandtll-number fluid flow is suppressed. The net effect is that a single thermal plume is observed to move in the direction opposite to that of the inner rotating cylinder. This thermal plume movement is distinctly different and opposite to that observed for

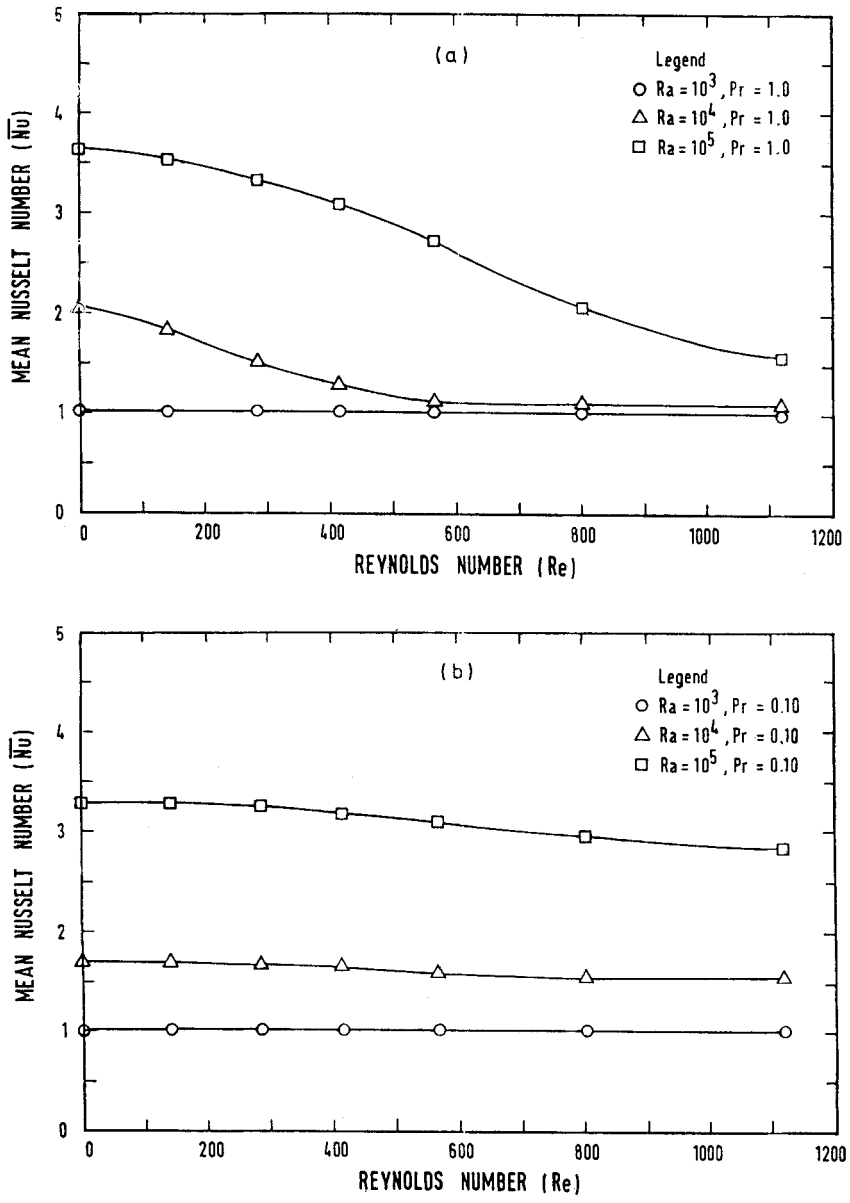

Figure 7. Effect of rotation of inner cylinder on mean Nusselt number at various *Ra* (RR = 2·6): (a) *Pr* = 1·0; (b) *Pr* = 0·1; (c) *Pr* = 0·01

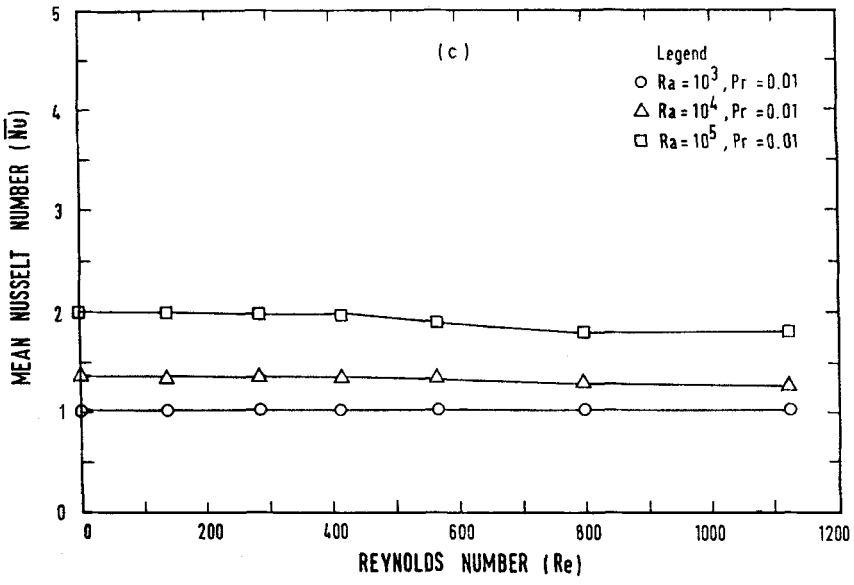

Figure 7. (Continued)

high-Prandtl-number fluid flow, where the monothermal plume on top of the inner cylinder moves in the same direction as the rotation of the inner cylinder.

The corresponding effect of increasing the rotational speed of the inner cylinder on the mean Nusselt number with varying Rayleigh and Prandtl numbers is shown in Figure 7. The general trend is that at higher Prandtl and Rayleigh numbers (Figure 7(a)) the mean Nusselt number falls with increasing rotational speed of the inner cylinder. The drop in the value of mean Nusselt number was also visualized with the aid of the streamline and temperature contours in the numerical experiments. At high rotational rate (i.e. high Re) the thermal plume formed by natural convective motion above the inner cylinder gradually disappeared. The isothermals near the inner cylinder gradually formed into concentric rings and the isotherm spacing gradually increased, indicating a drop in temperature gradient and hence a drop in mean Nusselt number. When eccentricity is introduced, the general trend is that the mean Nusselt number falls off from its stationary value with increasing rotational Reynolds number in a manner similar to the behaviour of the concentric case.

For the case of low Prandtl numbers of 0·1–0·01 Figures 7(b) and 7(c) show that as the Rayleigh number increases, the overall equivalent thermal conductivity increases. This is expected since the mode of heat transfer changes from conduction to convection as the Rayleigh number increases. However, at a particular Rayleigh number the variation in the overall equivalent thermal conductivity is negligible when the Reynolds number is increased. For the case of a Rayleigh number of 10^3 and a Prandtl number of 0·01 the overall equivalent thermal conductivity varies from a minimum of 1·02 at a Reynolds number of 140 to a maximum of 1·10 at a Reynolds number of 1120. The value of the overall thermal conductivity approaches 1·0, indicating that the mode of heat transfer is essentially conduction. When the Rayleigh number was increased to 10^5, it was noted that the overall thermal conductivity varies between a maximum value of 2·01 and a minimum value of 1·80. From the above studies it can be concluded that

for a given Rayleigh number in the range 10^3–10^6 the overall equivalent thermal conductivity is almost constant for low-Prandtl-number fluids when the inner cylinder is made to rotate in the Reynolds number range 0–10^3, though the streamlines, isotherms and local equivalent thermal conductivities exhibit very different features.

CONCLUSIONS

For the range of Prandtl numbers considered here, numerical experiments show that the mean Nusselt number increases with increasing Rayleigh number for both concentric and eccentric stationary inner cylinders. At a Prandtl number of order 1·0 with a fixed Rayleigh number, when the inner cylinder is made to rotate, the mean Nusselt number decreases throughout the flow. Although the flow pattern observed in this study varies significantly with respect to the rotational Reynolds number at lower Prandtl numbers of the order 0·1–0·01 with a given Rayleigh number, the mean Nusselt number remains fairly constant with respect to the rotational Reynolds number.

ACKNOWLEDGEMENTS

The author gratefully acknowledges the financial support of a National University of Singapore Research Grant (No. RP890633) and the assistance of S. Y. Lim, T. H. Tan, K. S. Yeo and C. L. Soh during the course of this work.

APPENDIX: NOMENCLATURE

$\mathbf{g}$	gravitational vector
L	characteristics length $L=R_o-R_i$
M, N	mesh sizes
Nu	local Nusselt Number
$\overline{Nu}$	mean Nusselt Number
∇P	pressure gradient
Pr	Prandtl Number, $Pr=\nu/\alpha$
r	radial co-ordinate
R_i, R_o	inner and outer cylinder radii
RR	radius ratio, $RR=R_o/R_i$
Ra	Rayleigh Number, $Ra=\beta g L^3 T_m/\alpha\nu$
Re	rotational Reynolds number of inner cylinder, $Re=R_i\omega L/\nu$
$t, \Delta t$	time and time increment
T	temperature
T_i, T_o	temperatuers of inner and outer cylinders
T_R	reference temperature, $T_R=(T_i+T_o)/2$
T_m	$T_i-T_o/2$
u	radial velocity
v	tangential velocity

Greek letters

α	thermal diffusivity or angular position of eccentricity vector ε measured anticlockwise from downward vertical of gravitational vector through centre of heated cylinder

β thermal coefficient of volumetric expansion or $\partial\eta/\partial r^*$ in transformed solution domain
ε eccentricity, i.e. distance between centres of inner and outer cylinders
ε_h horizontal eccentricity (positive to right)
ε_v vertical eccentricity (positive upwards)
η dimensionless transformed radial co-ordinate, $\eta=(r-r_i)/(r_o-r_i)$
θ dimensionless temperature, $\theta=(T-T_R)/T_m$
ϕ angular co-ordinate of original solution region measured from downward vertical through centre of outer cylinder
γ angular co-ordinate of transformed solution region measured from reference angle ϕ_c from vertical through centre of outer cylinder, $\gamma=\phi-(\phi_c-\alpha)$
κ, λ $\partial\eta/\partial\phi$, $\partial^2\eta/\partial\phi^2$ respectively in transformed co-ordinates
ν kinematic viscosity
ρ reference density corresponding to T_R
ϕ angular co-ordinate
ω_i angular velocity of inner rotating cylinder (positive anticlockwise)
ψ streamfunction
ζ vorticity

REFERENCES

1. T. H. Kuehn and R. J. Goldstein, 'An experimental and theoretical study of natural convection in the annulus between horizontal concentric cylinders', *J. Fluid Mech.*, **74,** 695–719 (1976).
2. T. H. Kuehn and R. J. Goldstein, 'An experimental study of natural convection heat transfer in concentric and eccentric horizontal cylindrical annuli', *ASME J. Heat Transfer*, **100,** 635–640 (1978).
3. D. W. Pepper and R. E. Cooper, 'Numerical solution of natural convection in eccentric annuli', *AIAA Paper 82-0983*, 1982.
4. R. F. Babus'Haq, S. D. Probert and M. J. Shilston, 'Natural convection across cavities: design advice', *Appl. Energy*, **20,** 161–188 (1985).
5. M. A. Hessami, A. Pollard, R. D. Powe and D. W. Ruth, 'A study of free convective heat transfer in a horizontal annulus with large radii ratio', *J. Heat Transfer*, **107,** 603–610 (1985).
6. E. K. Glakpe, C. B. Watkins and J. N. Cannon, 'Constant heat flux solutions for natural convection between concentric and eccentric horizontal cylinders', *Numer. Heat Transfer*, **10,** 279–295 (1986).
7. E. H. Bishop and S. C. Brandon, 'Heat transfer by natural convection of gases between horizontal isothermal concentric cylinders: the expansion number effect', *ASME–JSME Thermal Engineering Joint Conf., Vol. 2*, 1989, pp. 275–280.
8. A. Castrejon and D. B. Spalding, 'An experimental and theoretical study of transient free-convection flow between horizontal concentric cylinders', *Int. J. Heat Mass Transfer*, **31,** 273–284 (1988).
9. E. H. Bishop, 'Heat transfer by natural convection of helium between horizontal isothermal concentric cylinders at cryogenic temperatures', *J. Heat Transfer*, **110,** 109–115 (1988).
10. M. A. Hessami, G. De Vahl Davis, E. Lenonardi and J. A. Reizes, 'Mixed convection in vertical cylindrical annuli', *Int. J. Heat Mass Transfer*, **30,** 151–161 (1987).
11. S. V. Randriamampiania, A. P. Bontoux and B. Roux, 'Boundary driven flows in rotating cylindrical annulus', *Int. J. Heat Mass Transfer*, **30,** 1275–1286 (1987).
12. T. S. Lee, 'Free and forced convection in concentric and eccentric horizontal cylindrical annuli', *Proc. ASME/JSME Thermal Engineering Joint Conf., Vol. 3*, Honolulu, HW, March 1983, pp. 125–131.
13. T. S. Lee, 'Numerical experiments with laminar fluid convection between concentric and eccentric heated rotating cylinders', *Numer. Heat Transfer*, **7,** 77–87 (1984).
14. T. S. Lee, N. E. Wijeysundera and K. S. Yeo, 'Free convection fluid motion and heat transfer in horizontal concentric and eccentric cylindrical collector systems', *Proc. ASME Solar Energy Division Sixth Ann. Conf.*, Las Vegas, NV, 1984, pp. 194–200.
15. T. S. Lee and C. L. Soh, 'Computational and experimental studies of convective heat transfer and fluid flow in eccentric annuli of rotating cylinders', *Proc. 3rd Australasian Conf. on Heat and Mass Transfer*, Melbourne, 1985, Research Publications Pte Ltd. Melbourne, Australia, 1985, pp. 17–24.
16. T. S. Lee, 'Laminar fluid convection of varying Prandtl number in the annuli of rotating cylinders', *Proc. 9th Australasian Fluid Mechanics Conf.*, Auckland, December 1986, The University of Auckland, Auckland, New Zealand, 1986, pp. 90–92.

17. T. S. Lee and K. S. Yeo, 'Laminar fluid convection of low Prandtl number fluid in annuli of rotating cylinders', *Proc. 10th Australasian Fluid Mechanics Conf., Vol. 1*, Melbourne, 1989, Research Publications Pte Ltd. Melbourne, Australia, 1989, pp. 45–48.
18. F. Ladeinde, 'Studies of thermal convection in self-gravitating and rotating horizontal cylinders in a vertical gravity field', *Ph.D. Thesis*, Cornell University, Ithaca, NY, 1988.
19. M. Prud'homme and L. Robillard, 'Natural convection in an annular fluid layer rotating at weak angular velocity', *Proc. 4th Int. Symp. on Transport Phenomena, Heat and Mass Transfer*, Sydney, July 1991, The University of New South Wales, Sydney, Australia, 1991.
20. H. Q. Yang, K. T. Yang and J. R. Lloyd, 'Natural convection suppression in horizontal annuli by azimuthal baffles', *Int. J. Heat Mass Transfer*, **31,** 2123–2135 (1988).
21. H. Q. Yang, K. T. Yang and J. R. Lloyd, 'Rotational effects on natural convection in a horizontal cylinder', *AIChE J.*, **34,** 1627–1633. (1988).
22. S. R. M. Gardiner and R. H. Sabersky, 'Heat transfer in annular gap', *Int. J. Heat and Mass Transfer*, **21,** 1459–1466 (1978).
23. M. Singh and S. C. Rajvanshi, 'Heat transfer between eccentric rotating cylinders', *J. Heat Transfer*, **102,** 347–350 (1980).
24. T. Fusegi, B. Farouk and K. S. Ball, 'Mixed-convection flows within a horizontal concentric annulus with a heated rotating inner cylinder', *Numer. Heat Transfer*, **9,** 591–604 (1986).
25. A. C. Ratzel, C. E. Hickox and D. K. Gartling, 'Technique of reducing thermal conduction and natural convection heat losses in annular receiver geometries', *J. Heat Transfer*, **101,** 108–113 (1979).
26. U. Projahn, H. Reiger and H. Beer, 'Numerical analysis of laminar natural convection between concentric and eccentric cylinders', *J. Numer. Heat Transfer*, **4,** 131–146 (1981).
27. P. J. Roache, *Computational Fluid Dynamics*, Hermosa, Albuquerque, NM, 1973.
28. D. W. Peaceman and H. H. Rachford, 'Numerical solution of parabolic and elliptic differential equations', *J. Soc. Indust. Appl. Math.*, **3,** 28–41 (1955).
29. S. McKee and A. R. Mitchell, 'Alternating direction methods for parabolic equations in two space dimensions with mixed derivatives', *Comput. J.* **13,** 81–86 (1970).
30. G. D. Raithby and K. G. T. Holland, 'A general method of obtaining approximate solutions to laminar and turbulent free convection problems', *Adv. Heat Transfer*, **11,** 265–315 (1975).